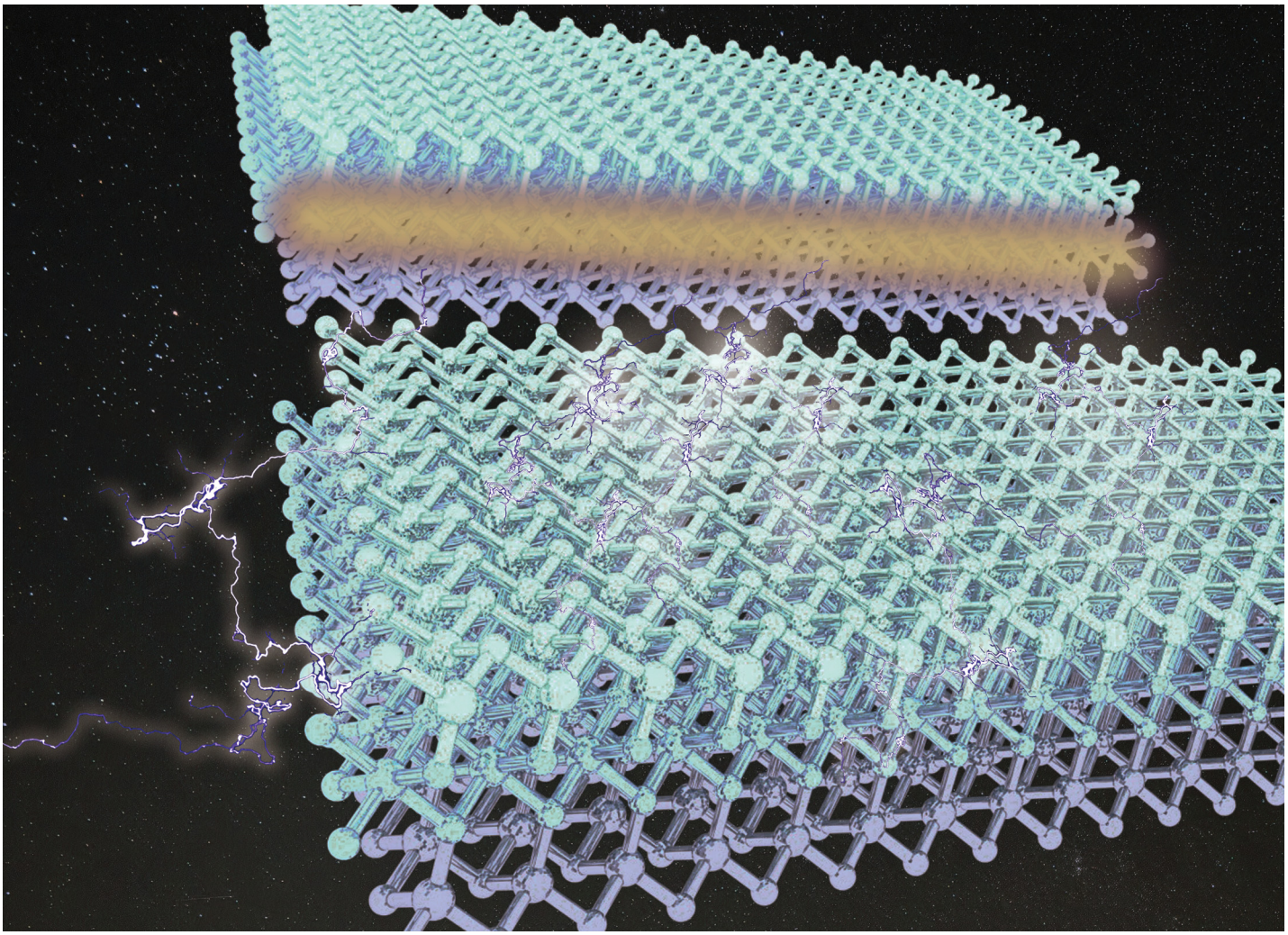

Showcasing research from the group of Prof. Hong Zhang at Sichuan University, China

Ideal two-dimensional quantum spin Hall insulators MgA_2Te_4(A = Ga, In) with Rashba spin splitting and tunable properties

This work investigates the MgA_2Te_4(A = Ga, In) family of two-dimensional quantum spin Hall insulators based on the in-depth first-principles calculations. With the inversion asymmetry, the Rashba spin splitting emerges and the two different types (Rashba-like and Dirac-type) of edge states along (010) occur for $MgGaInTe_4$. The bandgap and topological states can be modulated from the nontrivial to the trivial state by the electric field. The MgA_2Te_4(A = Ga, In) family has an outstanding potential to apply for the topological quantum field-effect transistors.

As featured in:

See Hong Zhang *et al.*, *Phys. Chem. Chem. Phys.*, 2024, **26**, 3815.

ROYAL SOCIETY OF CHEMISTRY

rsc.li/pccp

Registered charity number: 207890

PCCP Owner Societies

PCCP

ROYAL SOCIETY OF CHEMISTRY

PAPER

View Article Online
View Journal | View Issue

Cite this: *Phys. Chem. Chem. Phys.*, 2024, **26**, 3815

Ideal two-dimensional quantum spin Hall insulators MgA_2Te_4 (A = Ga, In) with Rashba spin splitting and tunable properties†

Jiaqi Li, [ab] Xinlu Cheng[c] and Hong Zhang *[ab]

Received 10th October 2023,
Accepted 6th December 2023

DOI: 10.1039/d3cp04898e

rsc.li/pccp

For decades, topological insulators have played a pivotal role in fundamental condensed-matter physics owing to their distinctive edge states and electronic properties. Here, based on in-depth first-principles calculations, we investigate the MgA_2Te_4 (A = Ga, In) structures belonging to the MA_2Z_4 2D material family. Among them, the topological insulator $MgGaInTe_4$ exhibits band inversion and a sizeable bandgap of up to 60.8 meV which satisfies the requirement for room-temperature realization. Under the spin–orbit coupling effect, $MgGaInTe_4$ with inversion asymmetry undergoes Rashba spin splitting. The Rashba-like and Dirac-type edge states emerge from different terminals along (010) for $MgGaInTe_4$. The external vertical electric field is verified to modulate the inverted bandgap and topological state of $MgGaInTe_4$ by converting a nontrivial state to a trivial state and $MgIn_2Te_4$ with the original trivial state to a nontrivial one. Accordingly, $MgGaInTe_4$ and $MgIn_2Te_4$ have significant potential for application in topological quantum field-effect transistors. Our research identifies that the MgA_2Te_4 (A = Ga, In) structures have huge potential to be candidate 2D materials for spintronics and topological quantum devices.

Introduction

2D topological insulators (TIs), also called quantum spin Hall insulators (QSHs), have attracted considerable attention due to their unusual quantum states with edge states different from conventional insulators. The topological nontrivial state can be classified by a Z_2 invariant which is a topological order parameter.[1,2] The appearance of this state is ensured by time-reversal symmetry which can impede backscattering, giving rise to highly active transport without dissipation.[3] The novel properties of these materials enable them to be used in various promising applications and fields, such as spintronics, low-dissipation electronic devices and quantum computing. On account of the features in convenient integration, 2D materials are more appropriate candidates than 3D TIs, which can be manufactured as good high-density and high-performance storage and logic devices.[4,5] As the first theoretically predicted one, the QSH effect in graphene is limited in observation under a theoretical temperature of 0.01 K, owing to its small bandgap and weak spin–orbit coupling (SOC).[6] In terms of the experiment, the HgTe/CdTe quantum well was first certified as a 2D TI with a tiny bandgap corresponding to low temperature, hampering the application at room temperature. The measured phenomenon is two edge states with opposite spins propagating in opposite directions. This topological nontrivial state appears only when the quantum well achieves a critical thickness.[7,8] The special edge states are the key feature of the TIs. Therefore, a distinctive edge state has gained much attention. Yan *et al.* found that the topological Shockley surface states on many noble metals (Au, Ag, Cu, Pt, and Pd) are entangled resembling Rashba-splitting.[9] In the occupied states of As(1 1 1), the surface state presents nearly-free electron (NFE) band dispersion affected by the Rashba effect.[10]

Recently, monolayers $MoSi_2N_4$ and WSi_2N_4 have been experimentally synthesized by chemical vapor deposition (CVD).[11] As a novel family of 2D materials, MA_2Z_4 has been surveyed theoretically.[12–19] The septuple-atomic-layer structure makes it possible to have different types of derivatives. The systems with diverse valence electrons have been predicted to be thermodynamically and dynamically stable. Among them, (Ca, Sr)Ga_2Te_4 and $SrGa_2Se_4$ are topologically nontrivial insulators.[12,13] In addition, $VN_2X_2Y_2$ nanosheets (X = B–Ga and Y = O–Te) show the quantum anomalous Hall state under critical strain.[14] Several MA_2Z_4 members exhibit an enormous Rashba effect enabling them for application in electronics and spintronics.[16] Wang *et al.*[13] only presented a nonzero topological invariant of β2-$MgGa_2Te_4$. However, the respective edge state was not given.

[a] *College of Physics, Sichuan University, Chengdu 610065, China. E-mail: hongzhang@scu.edu.cn*
[b] *Key Laboratory of High Energy Density Physics and Technology (Ministry of Education), Sichuan University, Chengdu 610065, China*
[c] *Institute of Atomic and Molecular Physics, Sichuan University, Chengdu 610065, China*

† Electronic supplementary information (ESI) available. See DOI: https://doi.org/10.1039/d3cp04898e

The spin properties and states of quantum matter for the MgA_2Te_4 family are not clear yet. Hence, it is necessary to investigate the topological and electronic properties of MgA_2Te_4 (A = Ga, In) which can provide theoretical guidance.

The outline of this work is as follows. We predict the stability of $MgGaInTe_4$ with phonon dispersion and *ab initio* molecular dynamics (AIMD) simulations. The SOC effect leads to a bulk gap of up to 60.8 meV which is larger than the energy scale of room temperature. Furthermore, it exhibits large Rashba-splitting. Interestingly, a strong hexagonal warping effect appears in the valence band close to the gamma point which gives rise to nonzero out-of-plane spin polarization S_z. Then, the topological nontrivial states are doubly identified by the Z_2 topological invariant. Moreover, we discovered an intriguing topological edge state of $MgGa_2Te_4$ and a normal insulator $MgIn_2Te_4$. Accordingly, it is possible to realize the transition between the TI and the normal insulator (NI) using effective methods like an external vertical electric field. We utilize the electric field to tune the inverted bandgap and the topological state transition. Our research exhibits distinctive characteristics and significant potential in topology and spintronic devices.

Computational methods

This research study was all based on density functional theory using the Vienna Ab initio Simulation Package (VASP 5.4).[20] For exchange–correlation interactions, we utilize the Perdew–Burke–Ernzerhof generalized gradient approximation (PBE-GGA)[21] with projector-augmented wave (PAW) pseudopotential. Derived from the study[11] relevant to the $MoSi_2N_4$ monolayer that the experimental bandgap (1.94 eV) is much closer to the GGA gap (1.744 eV) than the HSE gap (2.297 eV), we choose the GGA for exchange and correlation functions similar to that for the Janus MA_2Z_4 monolayer. The plane-wave cutoff energy for self-consistent and electronic calculations was 500 eV in a gamma-centred 12 × 12 × 1 k mesh for the Brillouin zone. For structural optimization calculations, the structures are fully optimized until the forces on each atom were less than 0.0001 eV $Å^{-1}$ with an energy convergence threshold of 10^{-8} eV. The vacuum was over 25 Å for 2-dimensional materials used to avoid interlayer interactions. The phonon dispersion is calculated using the density functional perturbation theory by Phonopy code in a 5 × 5 × 1 supercell. The *ab initio* molecular dynamics simulations were implemented with a Nose–Hoover thermostat at a room temperature of 300 K with a time step of 3 fs. The spin texture with constant energy contour was plotted using the PYPROCAR code.[22] The tight-binding Hamiltonians were calculated using the maximally localized Wannier functions using the WANNIER90 package.[23] Moreover, the topological properties were calculated using the WANNIERTOOLS package.[24]

Results and discussion

A. Structure properties

The fully optimized structure is the β2 type of MA_2Z_4 family which can be decomposed into MoS_2-type MZ_2 and InSe-type A_2Z_2. The composite structure seems like the A_2Z_2 monolayer is cut off and inserted into a single MZ_2 layer. The diverse kinds of A_2Z_2 and MZ_2 make it possible to form several structures. There are two types for A_2Z_2 (α phase and β phase) and MZ_2 (1T phase and 2H phase). Among these compounds, the β2 type consists of the MZ_2 1T phase and A_2Z_2 β phase which has the lowest enthalpies of formation.[13] Fig. 1 shows the β2 $MgGaInTe_4$ substituting one Ga atom for one In atom which breaks the centrosymmetry in space from $MgGa_2Te_4$. After displacement, the symmetry group becomes $P3m1$. The reduced symmetry will bring about Rashba-splitting with the SOC effect. To further demonstrate the asymmetry of the structure, we implement planar average potential along the z-axis. On account of the difference in electronegativity and atomic radius, the diverse heights (h_1 and h_6; h_2 and h_5) between layers give rise to the asymmetry of planar average potential along the z direction (about 16 Å and 24 Å), which can induce Rashba-splitting. The height of each atom layer is given in Table 1. The lattice constant of $MgGaInTe_4$ is 4.369 Å between $MgGa_2Te_4$ (4.290 Å) and $MgIn_2Te_4$ (4.453 Å). In Fig. 1(b), the black dotted line displays the primitive cell.

B. Stability

To confirm the dynamic stability of the structure, the phonon spectrum is implemented. As depicted in Fig. 2(a), there is almost no imaginary frequency along the high symmetry path

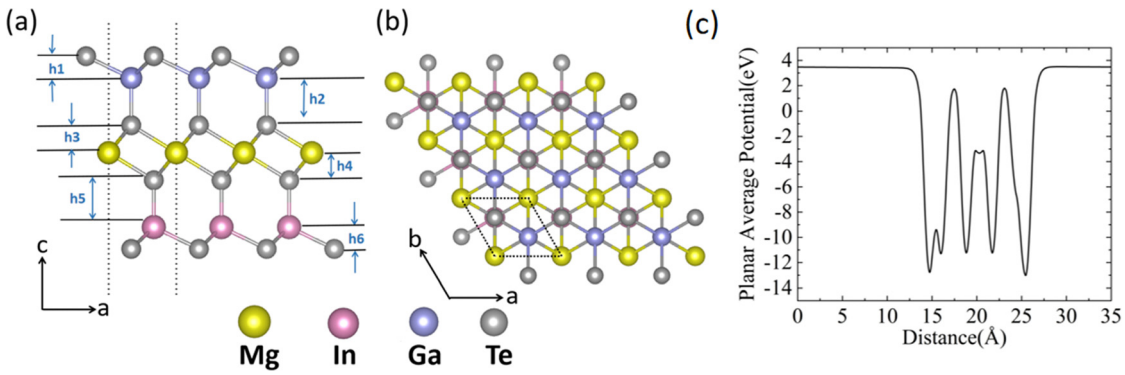

Fig. 1 Crystal structure of the $MgGaInTe_4$ monolayer in (a) side view with structure details and (b) top view with the primitive cell in the black dotted line and coordinate axes are marked. (c) Planar average potential along the z-axis shows the potential distribution.

Table 1 The structure parameter and mechanical properties of $MgGaInTe_4$

h_1 (Å)	h_2 (Å)	h_3 (Å)	h_4 (Å)	h_5 (Å)	h_6 (Å)	a (Å)
1.168	2.578	1.483	1.483	2.744	1.377	4.369
E_f (eV)	C_{11} (N m^{-1})	C_{12} (N m^{-1})	C_{66} (N m^{-1})	Y_{2D} (N m^{-1})	ν	
−3.184	73.623	26.413	23.605	64.147	0.359	

which indicates that the $MgGaInTe_4$ monolayer is dynamically stable. In three acoustic modes, when the k vector is close to the gamma point, two branches display linear dependency representing the in-plane motion. Another mode with a lower frequency is the ZA branch related to the out-of-plane motion which exhibits quadratic dispersion as k approaches 0. The phenomena mentioned above are the characteristics of 2D materials.[25–28] The thermal stability can be evaluated from the *ab initio* molecular dynamics (AIMD) simulation. In Fig. 2(b), the total energy fluctuates within a certain range as a function of simulation time at 300 K. As depicted in Fig. 2(b), the left panel displays the top view and the right panel shows the side view of the 4 × 4 × 1 supercell after a simulation time of 9000 fs. It is worth noting that the structure emerges with almost no reconstruction which corroborates the thermal stability of the $MgGaInTe_4$ monolayer.

In terms of mechanical stability, the elastic constants C_{ij} are calculated using the energy-strain method, as shown in Table 1. Owing to the hexagonal symmetry of 2D materials, the elastic matrix is transformed by the Voigt notation ignoring the thickness along the z-axis, which obtains the matrix elements C_{11}, C_{12} and C_{66}.[29] The C_{66} is equal to $(C_{11} - C_{12})/2$, also called a shear modulus. The Born criteria declare a structure to be mechanically stable as long as $C_{11} > 0$ and $C_{66} > 0$. The C_{11} is 73.623 N m^{-1}, and the C_{66} is 23.605 N m^{-1}. Consequently, it proves the mechanical stability of the $MgGaInTe_4$ monolayer. Besides, the Young modulus Y_{2D} is 64.147 N m^{-1}, one order smaller than graphene (342 N m^{-1})[30] and the Poisson ratio ν is relatively low. Therefore, this illustrates that the $MgGaInTe_4$ monolayer lacks in-plane stiffness, though it is soft enough to apply biaxial strain for tuning the properties of the material. In addition, the formation energy (E_f) of $MgGaInTe_4$ is −3.184 eV per atom as shown in Table 1. The formula of formation energy (E_f) is defined as below:

$$E_f = \left(E_{tot} - \sum N_i \times E_i\right) \Big/ N_{tot} \quad (1)$$

where E_f, E_{total} and E_i represent the energy of the formation process, the total energy of $MgGaInTe_4$, and the energy of each isolated atom, respectively. N_i and N_{tot} stand for the number of each kind of atom and the number of all atoms, respectively. The negative E_f (−3.184 eV) is small enough to prove the stability on the other hand which provides a large possibility of synthesis for the experiment.

C. Bulk electronic structure and Rashba splitting

With an eye towards the heavy elements In and Te, the effect of SOC is taken into account to accurately determine the VBM and CBM. The electronic structure of $MgGaInTe_4$ with GGA + SOC is depicted in Fig. 3(a) and the enlarged view exhibits obvious Rashba-splitting at the edge of the VBM. The most outstanding feature of the SOC effect is the existence of Rashba-splitting caused by the breaking of inversion symmetry rather than Dresselhaus spin-splitting.[31] To further identify Rashba spin splitting, the spin texture is implemented with the relevant energy constants of −0.075 eV below and +0.1 eV and +0.56 eV above the Fermi energy level. The spin-projected contour is centered at the gamma point in plane k_x–k_y. The S_x, S_y and S_z spin components are present in Fig. 3(b), (c) and (d), respectively. The colour bars on the right panels are leveraged to depict the spin projection strength, of which the red and blue colours stand for spin up and spin down, respectively. For all

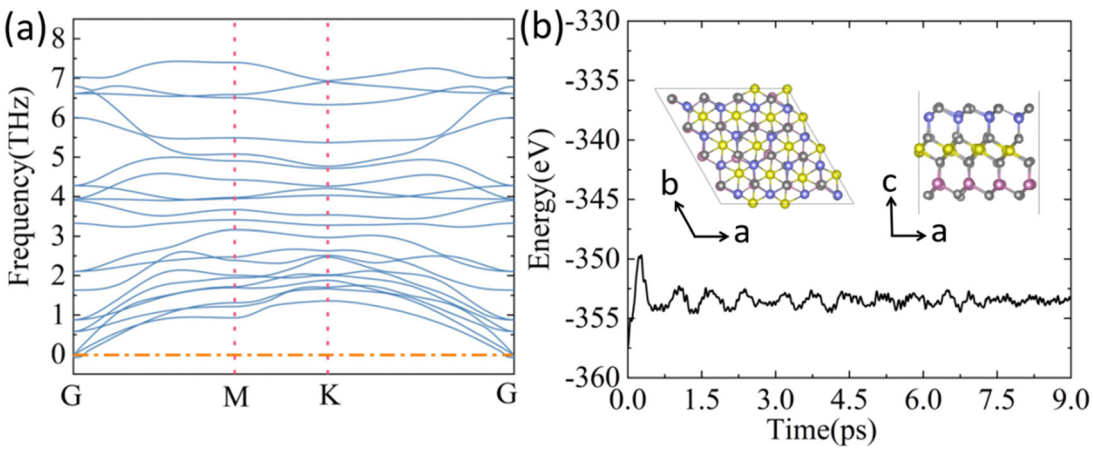

Fig. 2 (a) Phonon dispersion of the $MgGaInTe_4$ structure. (b) Total free energy of the $MgGaInTe_4$ monolayer with a time evolution of 9 ps and the supercell shows nearly no deformation after 9 ps. The molecular dynamics simulation is implemented at a temperature of 300 K.

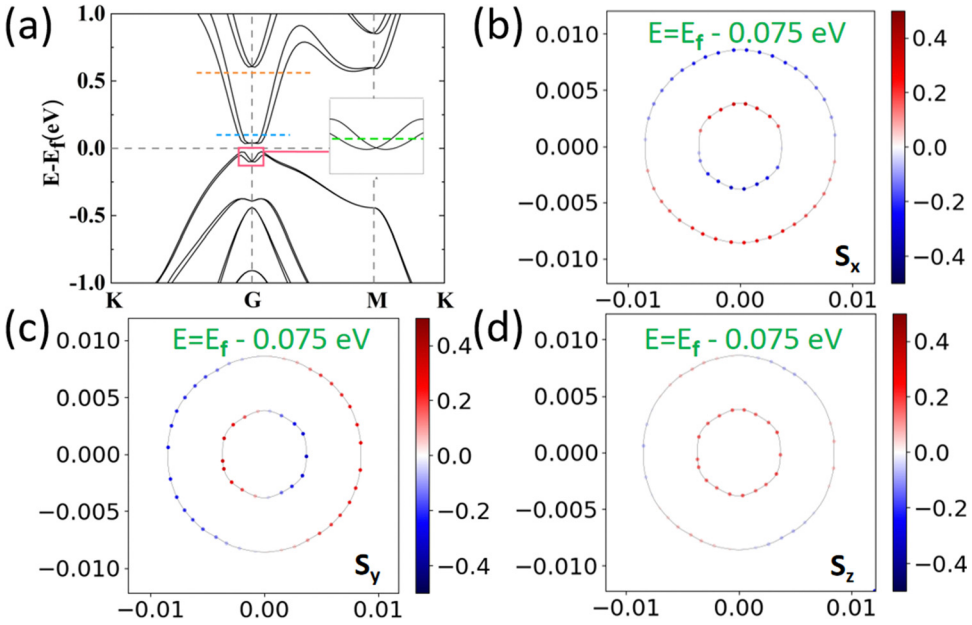

Fig. 3 (a) Rashba splitting in valence bands of $MgGaInTe_4$. (b)–(d) Spin texture in the *xy* plane centered at the gamma point of an energy criterion of −0.075 eV below the Fermi energy in the green line of (a). Red and blue colors represent spin up and spin down, respectively.

spin projections, a pair of closed circular lines are corresponding to the map of two top valence bands in terms of an energy criterion of −0.075 eV below the Fermi energy level (the green dotted line in Fig. 3(a)). A couple of circles observed with opposite chirality for in-plane spin projection (S_x and S_y) prominently confirms the presence of Rashba-type SOC. In addition, the out-of-plane spin projection S_z emerges at a low intensity. This demonstrates that almost only in-plane spin components exist. It enables a high efficiency for the applications of spin field-effect transistors. Consequently, the outstanding Rashba feature makes the $MgGaInTe_4$ a competitive candidate for nanoelectronics and spintronics.

In addition, Fig. 4 shows the energy contours of +0.1 eV and +0.56 eV above the Fermi energy (the blue and orange lines in Fig. 3(a)). The contour of a lower energy of +0.1 eV on conduction bands displays a group of chiral circles similar to valence bands in Fig. 3 proving the presence of Rashba splitting. Interestingly, the energy contours up to +0.56 eV in Fig. 4(d) show the rings not akin to circles, but rather hexagonal distortion in stark contrast to a circle. Conventional Rashba-type bands are relevant to a linear momentum k,[32] while hexagonal distortion in the in-plane chiral spin-texture originates from the hexagonal warping interaction depending on the k^3 terms. The nonparabolic band structure directly gives rise to the hexagonal distortion.[33]

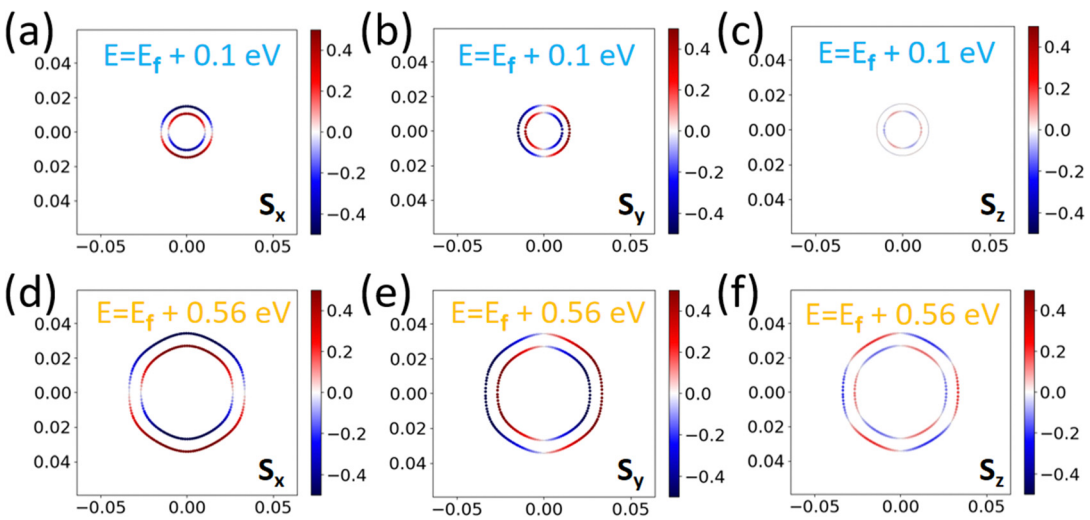

Fig. 4 Rashba splitting on conduction bands of $MgGaInTe_4$. (a)–(c) Spin texture in the *xy* plane centered at the gamma point of an energy criterion of +0.1 eV above the Fermi energy. (d)–(f) Spin texture in the *xy* plane centered at the gamma point of an energy criterion of +0.56 eV above the Fermi energy. The red and blue colors represent spin up and spin down, respectively.

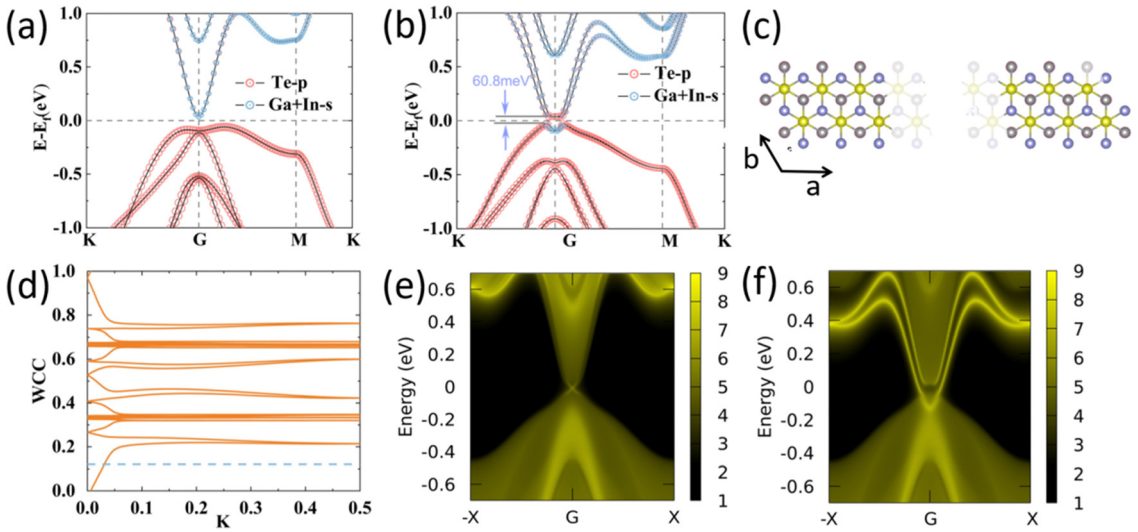

Fig. 5 (a) and (b) The orbital projection band without and with spin–orbit coupling for $MgGaInTe_4$, respectively. (c) Lattice structure of semi-infinite one-dimensional edges of $MgGaInTe_4$. The edges are along the *b*-axis and the period direction along the *a*-axis. (d) Wannier charge centers of $MgGaInTe_4$. (e) and (f) Left and right edge states, respectively. The electronic spectrum is calculated along the (010) edge.

This hexagonal distortion causes the non-zero out-of-plane spin projection S_z.[34]

D. Edge states and band inversion

To comprehend the preliminary properties of topological insulators, the band structures of $MgGaInTe_4$ with SOC and without SOC calculated by GGA are present in Fig. 4. The orbital-resolved band structures with and without SOC effects are shown in Fig. 5(a) and (b), respectively. Without SOC, it belongs to a normal insulator in which the CBM locates at the gamma point and the VBM locates along the gamma–*M* path with continuous orbital projections (Te-p, Ga-s, and In-s). In the case of SOC, the valence band and the conduction band approach each other and open a gap centered at the gamma point. The SOC triggers significant band gaps up to 60.8 meV, which is larger than the energy scale of room temperature. Therefore, it can be measured experimentally at room temperature and the material has potential for low-power electronic devices.[35] Furthermore, the continuous orbital projection bands are split and exchange the components in close proximity to the gamma point. A noticeable band inversion shown in Fig. 5(b) manifests that the *s* states of Ga and In lie below the p states of Te, strong hybridization between Ga, In and Te orbitals notwithstanding. The band inversion and noticeable open gap usually indicate the generation of the QSH state.[36]

To further delineate the nontrivial topology, we turn to obtaining the topological invariant Z_2 and conducting helical edge states to confirm a TI. Owing to the emergence of time-reversal symmetry, the TI can be verified by the Z_2 topological invariant as an authentic criterion for QSH insulators. The Z_2 number can be obtained according to the method of Fu and Kane[37] by calculating the parity eigenvalues of the occupied valence bands at time-reversal-invariant momentum (TRIM) points. Nevertheless, it is worth noting that this method is not suitable for $MgGaInTe_4$ attributed to the rupture of inversion symmetry. Another pathway is to implement the evolution of Wannier charge centers (WCCs).[38] The Z_2 number can be identified by the time that an arbitrary horizontal line crosses the pattern of WCCs. Wherever the horizontal line locates, the odd cross times correspond to $Z_2 = 1$. In contrast, the even times are on behalf of $Z_2 = 0$. As shown in Fig. 4(d), the reference dashed line in blue and the evolution WCCs intersect once. Hence, the topological invariant Z_2 equals 1 exemplifying a nontrivial state.

In addition, the topologically protected edge states of $MgGaInTe_4$ are present in Fig. 5(e) and (f). We research the (010) edge of the $MgGaInTe_4$ Janus monolayer along the *b*-axis including the left edge and the right edge. And, the *a*-axis represents the periodic direction. In virtue of inversion asymmetry, the material possesses different terminals (left and right edges) giving rise to different edge electronic states. The two edge states depict two sorts of dispersion: the Dirac-type edge state and the Rashba-type edge state. A linear dispersion in the vicinity of the Fermi energy appears in Fig. 5(e) (the left edge state). A pair of straight lines cross the connection between the conduction and valence bands. The Dirac-type band is characterized by the zero-effective mass of the carriers close to the Dirac cone with high Fermi velocity (up to 2.0×10^4 m s^{-1} for $MgGaInTe_4$). Such a linear relationship of electronic states reveals high transition efficiency from the bulk band to the edge state. A nonlinear dispersion links the conduction and valence bands in Fig. 5(f). The cross point is pushed up away from the Fermi energy and a displacement from the gamma point emerges at the *X* point. The curve resembles Rashba-like splitting in the bulk band (as shown in Fig. 5(b)). Compared to a classic Dirac-type cross, the intersecting point above the Fermi energy prompts the stability of the edge state.

Besides, the structures ($MgGa_2Te_4$ and $MgIn_2Te_4$) retaining inversion symmetry are also given in Fig. 6. As depicted in Fig. 6(a)–(c), under the SOC effect, the band of $MgGa_2Te_4$ only possesses the band inversion at the gamma point without Rashba splitting. Strikingly, the entangled Rashba-like edge

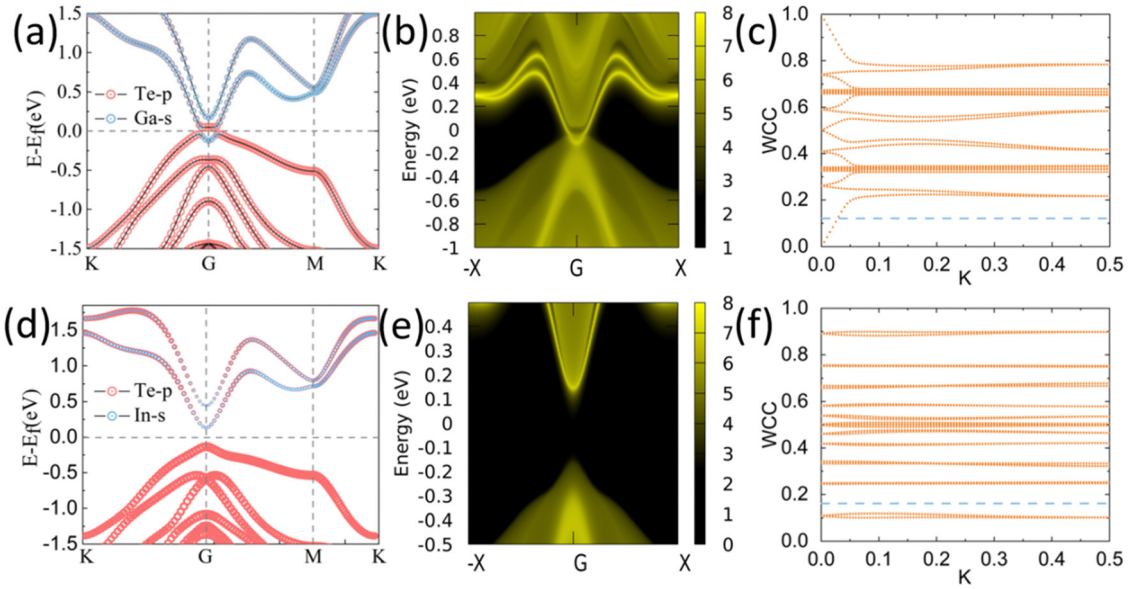

Fig. 6 The orbital projection band (a) with spin–orbit coupling, left edge state (b) and Wannier charge centers (c) of $MgGa_2Te_4$, respectively; the orbital projection band (d) with spin–orbit coupling, left edge state (e) and Wannier charge centers (f) of $MgIn_2Te_4$, respectively.

state arises in the nontrivial state (Z_2 = 1) in accord with the previous research study.[13] Deriving from keeping the inversion symmetry, the direction along (010) has the equivalent terminal for the left edge and the right edge. Hence, we just exhibit the left edge for the edge state; Fig. 6(c)–(e) delineate a trivial state (Z_2 = 0) of $MgIn_2Te_4$ without band inversion.

E. Electric field switching of topological states

Applying an external electric field is verified to be a significant pathway to tune the electronic properties and topological characters. On account of the band inversion with respect to the nontrivial state dominated by the p orbital of Te atoms and s orbital of Ga and In atoms, as depicted in Fig. 1(a), the Te atoms and the Ga and In atoms are obviously located at different atom layers in terms of 2D materials. Hence, the electric field perpendicular to the nanosheet plane possesses efficient tunability for the Janus MgA_2Te_4 (A = Ga, In) spatial structure. Therefore, we utilize the vertical electric field to realize the regulation of bandgap and the topological state switching. The positive direction of the electric field gets along the +z axis of the physical structure.

Fig. 7(a) and (b) demonstrate that at a certain range of tiny external electric fields, the bandgap, band type and Z_2 number relevant to the topological states are desired to be modulated. The yellow area is on behalf of the nontrivial state (Z_2 = 1) and the blank area represents the trivial state (Z_2 = 0). Noticeably, the band transitions occur from indirect to semimetallic or direct to semimetallic when the electric field strength achieves the critical value. The topological open gap located at the gamma point becomes gapless in this situation and the VBM and CBM move to the gamma point as a direct bandgap. For $MgGaInTe_4$, the increasing positive electric field amplifies the bandgap keeping the indirect gap and a nontrivial state. In contrast, the bandgap first decreases close to zero under a negative

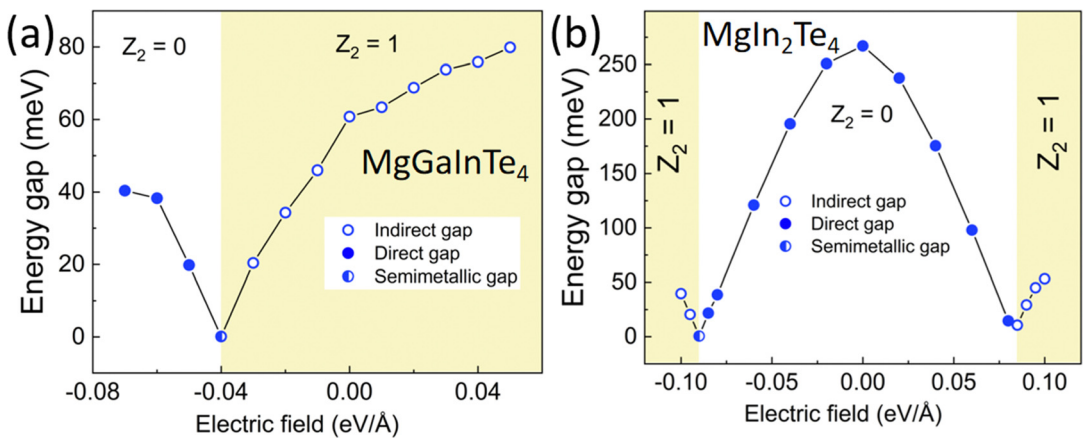

Fig. 7 Diagram of the bandgap as a function of external vertical electric field strength. The yellow area represents the nontrivial state (Z_2 = 1). The blank area is in the trivial state (Z_2 = 0). The different symbols represent different band types: (a) $MgGaInTe_4$ and (b) $MgIn_2Te_4$.

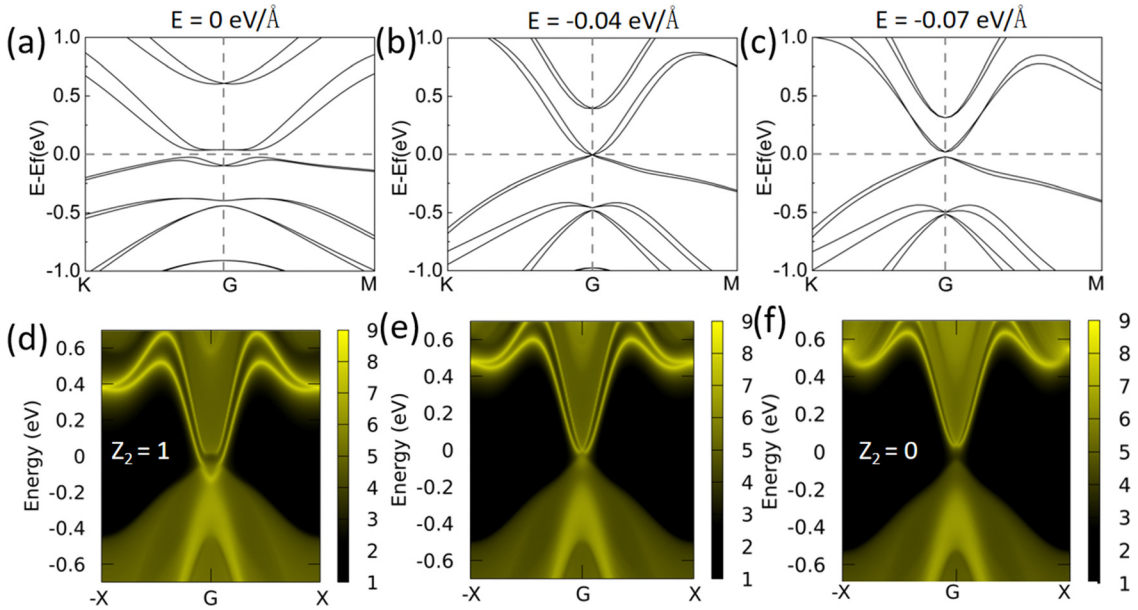

Fig. 8 The band structure of $MgGaInTe_4$ under different external electric fields and the right edge state along the direction (010). (a) and (d) Without the external electric field in the nontrivial state (b) and (e) for -0.04 eV Å^{-1} as a threshold and (c) and (f) for -0.07 eV Å^{-1} in the trivial state.

electric field. The critical electric field strength is -0.04 eV Å^{-1}. When the critical value is not up to -0.04 eV Å^{-1} or positive, the state remains nontrivial. While the electric field strength exceeds the critical value, the topological state is destroyed to trivial, switching off the QSH state. Equally, for $MgIn_2Te_4$ without an electric field, the Z_2 number is preliminarily zero. With the enhancement of the electric field, the bandgap decreases and it maintains the trivial state whether the field direction is positive or negative. Until attaining the critical strength (-0.09 eV Å^{-1} for the negative electric field and +0.085 eV Å^{-1} for the positive electric field), the state converts trivial to nontrivial.

In terms of the topological switching process, we exhibit the detail of state transition of $MgGaInTe_4$. Without an electric field, the topological Rashba-like edge state connecting the conduction band and the valence band is clearly observed in Fig. 8(d). When the external electric field strength achieves the critical value (-0.04 eV Å^{-1}), a semimetal bandgap of the Dirac cone in close proximity to Fermi energy emerges. Under this field, the edge state is pushed up nearly digressing from the valence band. Until the electric field strength reaches -0.07 eV Å^{-1}, the bandgap gradually increases as a direct bandgap. Meanwhile, Fig. 8(f) reveals that the conduction band and the valence band are separated without connection, accessing the trivial state ($Z_2 = 0$). The evolution of the switching nontrivial state on–off depends on whether the electric field exceeds the threshold value. Accordingly, $MgGaInTe_4$ and $MgIn_2Te_4$ have significant potential to apply for the topological quantum field-effect transistors. The schematic application of $MgGaInTe_4$ for topological quantum field-effect transistors is exhibited in Fig. 9. With no electric field, the state remains nontrivial. The topological state exemplifies the "on" state. The conductance exists in the edge channel of the 2D material. Moreover, the conductance maintains topologically protected due to the topologically protected edge state. Hence, the conductance can avoid interference of impurities robustly arising from the topological protection.[39] While the external electric field achieves the threshold, the conductance vanishes and the nontrivial state switches "off".

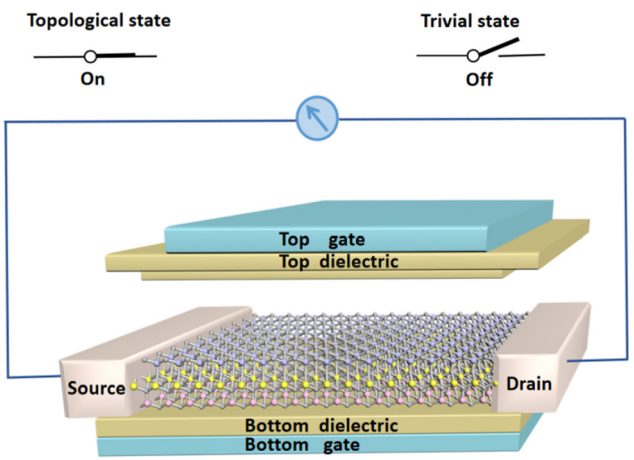

Fig. 9 Schematic diagram of topological quantum field-effect transistors using $MgGaInTe_4$. Without an electric field, the conductance of edge channels exists. The topological state represents "on." When the electric field reaches the threshold, the state converts to a trivial state, switching the topological state "off".

Conclusions

In summary, we demonstrate a candidate MgA_2Te_4 (A = Ga, In) family of 2D topological materials. Among them, $MgGaInTe_4$ and $MgGa_2Te_4$ are topological insulators, while $MgIn_2Te_4$ is the original trivial insulator. The dynamic and mechanical stabilities can be clarified by phonon dispersion, *ab initio* molecular dynamics simulations and elastic constants, respectively. $MgGaInTe_4$ has a bandgap of up to 60.8 meV higher than the

scale of room temperature which is beneficial to experimental room temperature realization. Owing to the inversion asymmetry and the SOC effect, the Rashba splitting is verified to emerge without the S_z spin component. The anisotropy of hexagonal distortion in large momentum k on the conduction bands arises from warping interaction depending on the k^3 terms. Furthermore, the band inversion is observed clearly and the topological insulator is confirmed by WCCs and the topological edge state. There is a lack of inversion symmetry and the terminals along (010) are different exhibiting Dirac and Rashba-type edge states. Besides, we utilize an external vertical electric field to modulate the bandgap and to realize the topological state transition. Strikingly, the nontrivial state of $MgGaInTe_4$ can be switched off to a trivial state provoked by a vertical electric field. Therefore, it is suitable for the application of topological quantum field-effect transistors. Interestingly, the preliminary $MgIn_2Te_4$ is topologically trivial with no electric field which can be converted to a nontrivial state by an electric field. Accordingly, $MgGaInTe_4$ and $MgIn_2Te_4$ indicate tremendous potential for employment in electronics and topological quantum field-effect transistors.

Conflicts of interest

There are no conflicts to declare.

Acknowledgements

This work was supported financially by the National Natural Science Foundation of China (11974253) and the Science Specialty Program of Sichuan University (Grand. No. 2020SCUNL210).

References

1 M. Z. Hasan and C. L. Kane, *Rev. Mod. Phys.*, 2010, **82**(4), 3045–3067.
2 X.-L. Qi and S.-C. Zhang, *Rev. Mod. Phys.*, 2011, **83**, 1057–1110.
3 Y. Wang, S. Lei, N. Wan, H. Yu and J. Chen, *Superlattices Microstruct.*, 2021, 107026.
4 X. Li, F. Liu and Q. Wang, *Phys. Rev. B*, 2020, **102**, 195420.
5 J. E. Moore, *Nature*, 2010, **464**, 194–198.
6 C. L. Kane and E. J. Mele, *Phys. Rev. Lett.*, 2005, **95**(22), 226801.
7 B. A. Bernevig, T. L. Hughes and S.-C. Zhang, *Science*, 2006, **314**, 1757–1761.
8 M. König, S. Wiedmann, C. Brüne, A. Roth, H. Buhmann, L. W. Molenkamp, X. L. Qi and S. C. Zhang, *Science*, 2007, **318**, 766–770.
9 B. Yan, B. Stadtmüller, N. Haag, S. Jakobs, J. Seidel, D. Jungkenn, S. Mathias, M. Cinchetti, M. Aeschlimann and C. Felser, *Nat. Commun.*, 2015, **6**, 10167.
10 P. Zhang, J. Z. Ma, Y. Ishida, L. X. Zhao, Q. N. Xu, B. Q. Lv, K. Yaji, G. F. Chen, H. M. Weng and X. Dai, *Phys. Rev. Lett.*, 2017, **118**, 046802.
11 Y. L. Hong, Z. Liu, L. Wang, T. Zhou, W. Ma, C. Xu, S. Feng, L. Chen, M. L. Chen, D. M. Sun, X. Q. Chen, H. M. Cheng and W. Ren, *Science*, 2020, **369**, 670–674.
12 L. Wang, Y. Shi, M. Liu, A. Zhang and X. Q. Chen, *Nat. Commun.*, 2021, **12**, 2361.
13 L. Wang, Y. Shi, M. Liu, Y. L. Hong, M. X. Chen, R. Li, Q. Gao, W. Ren, H. M. Cheng, Y. Li and X.-Q. Chen, *arXiv*, 2020, preprint, arXiv:2008.02981, DOI: 10.48550/arXiv.2008.02981.
14 Y. Wang and Y. Ding, *Appl. Phys. Lett.*, 2021, **119**, 193101.
15 S. D. Guo, W. Q. Mu, Y. T. Zhu, R. Y. Han and W. C. Ren, *J. Mater. Chem. C*, 2021, **9**(7), 2464–2473.
16 W. Zhou, L. Wu, A. Li, B. Zhang and F. Ouyang, *J. Phys. Chem. Lett.*, 2021, **12**, 11622–11628.
17 R. Islam, R. Verma, B. Ghosh, Z. Muhammad, A. Bansil, C. Autieri and B. Singh, *Phys. Rev. B*, 2022, **106**, 245149.
18 R. Islam, G. Hussain, R. Verma, M. S. Talezadehlari, Z. Muhammad, B. Singh and C. Autieri, *Adv. Electron. Mater.*, 2023, **9**, 2300156.
19 Y. Wang and Y. Ding, *Phys. Status Solidi RRL*, 2023, 2300376.
20 G. Kresse and J. Furthmüller, *Phys. Rev. B: Condens. Matter Mater. Phys.*, 1996, **54**, 11169–11186.
21 J. P. Perdew, K. Burke and M. Ernzerhof, *Phys. Rev. Lett.*, 1996, **77**, 3865–3868.
22 H. Mirhosseini, J. Henk, A. Ernst, S. Ostanin, C. T. Chiang, P. Yu, A. Winkelmann and J. Kirschner, *Phys. Rev. B: Condens. Matter Mater. Phys.*, 2009, **79**, 245428.
23 A. A. Mostofi, J. R. Yates, Y. S. Lee, I. Souza and N. Marzari, *Comput. Phys. Commun.*, 2008, **185**, 685–699.
24 Q. S. Wu, S. N. Zhang, H. F. Song, M. Troyer and A. A. Soluyanov, *Comput. Phys. Commun.*, 2017, S0010465517303442.
25 H. Zabel, *J. Phys. Condens. Matter*, 2001, **13**, 7679.
26 L. Zhu, G. Zhang and B. Li, *Phys. Rev. B: Condens. Matter Mater. Phys.*, 2014, **90**, 214302.
27 L. Jin, X. Zhang, Y. Liu, X. Dai, X. Shen, L. Wang and G. Liu, *Phys. Rev. B*, 2020, **102**, 125118.
28 Z. Zhu and D. Tomanek, *Phys. Rev. Lett.*, 2014, **112**, 176802.
29 R. C. Andrew, R. E. Mapasha, A. M. Ukpong and N. Chetty, *Phys. Rev. B Condens. Matter*, 2012, **85**(12), 125428.
30 C. Lee, X. Wei, J. W. Kysar and J. Hone, *Science*, 2008, **321**(5887), 385–388.
31 J. Schliemann, J. C. Egues and D. Loss, *Phys. Rev. Lett.*, 2003, **90**(14), 146801.
32 S. Singh and A. H. Romero, *Phys. Rev. B*, 2017, **95**, 165444.
33 S. Chen, Z. Zeng, B. Lv, S. Guo, X. Chen and H. Geng, *Phys. Rev. B*, 2022, **106**, 115307.
34 G.-Y. Chen, A. Huang, Y.-H. Lin, C.-J. Chen, D.-S. Lin, P.-Y. Chang, H.-T. Jeng, G. Bihlmayer and P.-J. Hsu, *npj Quantum Mater.*, 2020, **5**, 89.
35 S. S. Wang, W. Sun and S. Dong, *Phys. Chem. Chem. Phys.*, 2021, **23**(3), 2134–2140.
36 Q. Lu, B. Wang, X.-R. Chen and W.-M. Liu, *Phys. Rev. Mater.*, 2018, **2**, 014005.
37 L. Fu and C. L. Kane, *Phys. Rev. B: Condens. Matter Mater. Phys.*, 2007, **76**, 045302.
38 H. J. Monkhorst and J. D. Pack, *Phys. Rev. B: Solid State*, 1976, **13**, 5188–5192.
39 M. Ezawa, *J. Phys. Soc. Jpn*, 2015, **84**, 121003.

